applied sciences

MDPI

Article

Hydroxyl Radical Generation by the H_2O_2/Cu^{II}/Phenanthroline System under Both Neutral and Alkaline Conditions: An EPR/Spin-Trapping Investigation

Elsa Walger [1,*], Nathalie Marlin [1], Gérard Mortha [1], Florian Molton [2] and Carole Duboc [2]

[1] Institute of Engineering, University Grenoble Alpes, CNRS, Grenoble INP, LGP2, F-38000 Grenoble, France; nathalie.marlin@grenoble-inp.fr (N.M.); gerard.mortha@grenoble-inp.fr (G.M.)
[2] Department of Molecular Chemistry, University Grenoble Alpes, CNRS, DCM, F-38000 Grenoble, France; florian.molton@univ-grenoble-alpes.fr (F.M.); carole.duboc@univ-grenoble-alpes.fr (C.D.)
* Correspondence: elsa.walger@grenoble-inp.org

Abstract: The copper–phenanthroline complex $Cu^{I}(Phen)_2$ was the first artificial nuclease studied in biology. The mechanism responsible for this activity involves $Cu^{II}(Phen)_2$ and H_2O_2. Even if H_2O_2/Cu systems have been extensively studied in biology and oxidative chemistry, most of these studies were carried out at physiological pH only, and little information is available on the generation of radicals by the H_2O_2/Cu^{II}-Phen system. In the context of paper pulp bleaching to improve the bleaching ability of H_2O_2, this system has been investigated, mostly at alkaline pH, and more recently at near-neutral pH in the case of dyed cellulosic fibers. Hence, this paper aims at studying the production of radicals with the H_2O_2/Cu^{II}-Phen system at near-neutral and alkaline pHs. Using the EPR/spin-trapping method, $HO^{\bullet}$ formation was monitored to understand the mechanisms involved. DMPO was used as a spin-trap to form DMPO–OH in the presence of $HO^{\bullet}$, and two $HO^{\bullet}$ scavengers were compared to identify the origin of the observed DMPO–OH adduct, as nucleophilic addition of water onto DMPO leads to the same adduct. H_2O_2 decomposition was enhanced by the addition of Cu^{II}–Phen (and only slightly by addition of $CuSO_4$), reaching a level similar to the Fenton reagent at near-neutral pH. This evidences the role of Phen, which improves the effect of Cu^{II} by tuning the electronic structure and structural properties of the corresponding Cu^{II} complexes.

Keywords: copper-phenanthroline complex; EPR spectroscopy; hydrogen peroxide; hydroxyl radical; spin-trapping

Citation: Walger, E.; Marlin, N.; Mortha, G.; Molton, F.; Duboc, C. Hydroxyl Radical Generation by the H_2O_2/Cu^{II}/Phenanthroline System under Both Neutral and Alkaline Conditions: An EPR/Spin-Trapping Investigation. *Appl. Sci.* **2021**, *11*, 687. https://doi.org/10.3390/app11020687

Received: 1 December 2020
Accepted: 10 January 2021
Published: 12 January 2021

1. Introduction

In 1979, Cu^{+}(phenanthroline)$_2$ (the molecular structure of phenanthroline is presented in Figure 1) was discovered to display nuclease activity [1], by cleaving the phosphodiester bonds of DNA or RNA. The scission of DNA occurs in the presence of two co-reactants: Cu^{+}(phenanthroline)$_2$ and H_2O_2 [2,3]. According to Sigman [2], the Cu^{+}(phenanthroline)$_2$ complex coordinates to DNA and the oxidation of this coordinate by H_2O_2 further generates a cupric hydroxyl radical-like coordinate, responsible for the DNA scission.

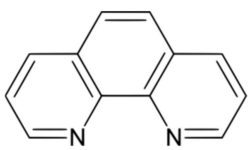

Figure 1. Molecular structure of 1,10-phenanthroline (Phen).

Hence, copper–phenanthroline coordinates (Cu–Phen) represent the first artificial nucleases studied in biology. Generally, they consist of bis(1,10-phenanthroline)copper(I) complexes [1–5], although a mono(1,10-phenanthroline)copper complex was found to

display better nuclease activity [6]. The active synthetic nucleases are commonly described as cuprous complexes. Chikira et al. evidenced the intercalative binding of the cupric Cu^{2+}(phenanthroline)$_2$ complex with DNA and attributed the DNA cleavage to this complex. Accordingly, the group of Liu has shown that cupric complexes could cleave DNA in the presence of H_2O_2 and a reductant, via a mechanism involving coordination of the copper(II) with DNA [7]. Even if it is also proposed that during the reaction several oxidized states of copper, from Cu^{II} to Cu^{III}, can be implicated [8], Cu^{II} reduction to Cu^{I} is involved in most cases [9].

The oxidation of lignin derivates with Cu–Phen complexes in the presence of H_2O_2 has been successfully investigated under alkaline conditions, demonstrating improved oxidative action compared to H_2O_2 alone [10,11]. The main application for such a system is in paper pulp bleaching. Under neutral conditions, this H_2O_2/Cu–Phen system also displayed activity in the decolorization of colored cellulosic fibers [12], reaching up to 50% color-stripping. However, this activity was accompanied by strong cellulose degradation that can be rationalized based on a radical mechanism via the decomposition of H_2O_2 into the highly oxidative hydroxyl radical, generated by the presence of Cu–Phen. The present study has been carried out in this context, especially on the color-stripping effect on dyed cellulosic fibers with H_2O_2/Cu–Phen at both near-neutral and alkaline pHs.

Hanna and Mason studied the formation of hydroxyl radicals by a Cu^{I}/H_2O_2 system [13] using the spin-trapping method based on EPR spectroscopy. This approach indirectly probes the presence of short-lived radical species, such as hydroxyl radicals, that react with a molecule called a spin-trap, to form a stable radical species detectable by EPR spectroscopy. Nitrones including 5,5-dimethyl-1-pyrroline N-oxide (DMPO, see Figure 2) are common spin-traps.

In the presence of hydroxyl radicals, DMPO forms the DMPO–OH adduct, which gives a typical four-line signal (Figure 2), with hyperfine splitting constants $a_N = a_H =$ 14.9 G. [14]

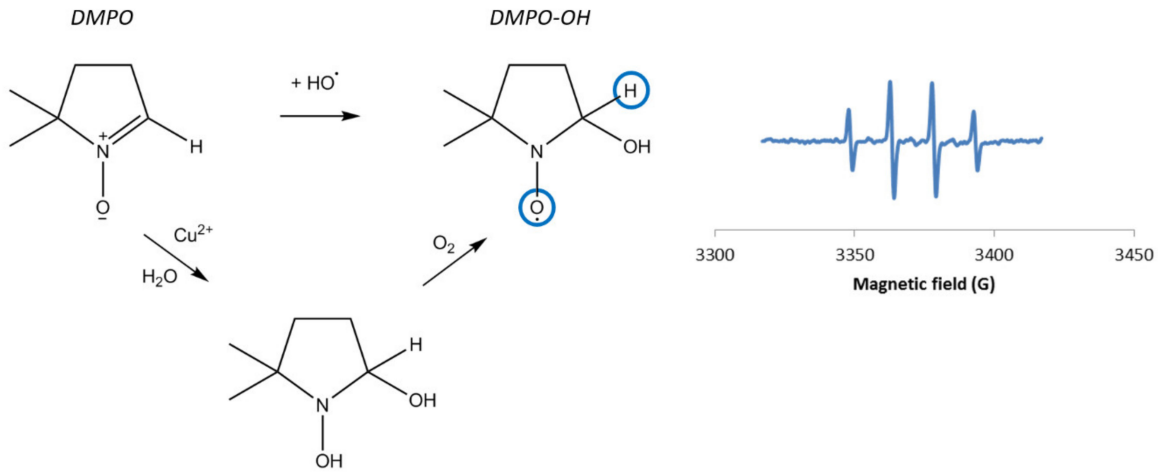

Figure 2. Left: Hydroxylation of DMPO into DMPO–OH and mechanism of nucleophilic addition of water on DMPO in the presence of Cu, also leading to the DMPO–OH adduct, as described by Burkitt et al. [15]; Right: Typical EPR spectrum of DMPO–OH [14,16,17].

However, the observation of DMPO–OH does not necessarily mean that HO• radicals are formed. Indeed, several phenomena lead to the DMPO–OH adduct, including (i) superoxide radical spin-trapping and decomposition of the corresponding DMPO–OOH adduct into DMPO–OH; (ii) the oxidation of DMPO by very strong oxidants (called inverted spin-trapping) [18]; or (iii) the nucleophilic addition of water onto the DMPO spin-trap (Forrester-Hepburn reaction) [19]. Besides, the nucleophilic addition of water is quite usual in aqueous solution and has been proved to be catalyzed by copper ions [13,15,20]. In the

case of Cu(II), the metal binds to DMPO and the polarization of the DMPO's double bond promotes the nucleophilic attack of H_2O (Figure 2).

To confirm that the observed DMPO–OH adduct originates from $HO^{\bullet}$ addition and not from these above-mentioned side reactions, an indirect method using scavenger molecules can be applied. The selected scavengers should be more reactive towards hydroxyl radicals than DMPO (rate constants higher than that of the spin-trap, k(DMPO/$HO^{\bullet}$)) and could be added at high concentrations. Among scavengers, dimethyl sulfoxide (DMSO) and formate ($HCOO^-$) are often used, and the resulting adducts are DMPO-$CH_3^{\bullet}$ with a typical six-line signal (a_N = 16.1 G, a_H = 23 G) and DMPO–$COO^{\bullet -}$ with another six-line pattern (a_N = 15.75 G, a_H = 19.09 G), see Figure S1 (Supplementary Materials).

While the spin-trapping technique has been extensively used to study hydroxyl radical formation by H_2O_2/Cu(I) [15] and H_2O_2/Cu(II) systems [21] especially in biology at physiological pH, less information is available when alkaline solutions are considered. In this context, this paper deals with the investigation of the decomposition of hydrogen peroxide into hydroxyl radicals in the presence of copper(II)–phenanthroline complexes in both neutral and alkaline aqueous media.

2. Materials and Methods

2.1. Analysis Conditions

The spin-trapping trials were carried out in aqueous solution at room temperature, except for some exceptional assays with heating.

2.1.1. Chemical Preparation

The commercial chemical products of analytical grade were DMPO 5,5-dimethyl-1-pyrroline N-oxide (99%, Sigma Aldrich, St. Louis, MO, USA), dimethyl sulfoxide (99.9%, Sigma Aldrich), and sodium formate HCOONa (99%, Carl Roth). The other chemicals were NaOH (99%, reagent grade, Carl Roth, Karlsruhe, Germany), hydrogen peroxide (35%, Carl Roth), copper sulfate $CuSO_4 \bullet 5H_2O$ (98.0%, Merck, Darmstadt, Germany), and 1,10-phenanthroline (99.0%, Acros Organics, Geel, Belgium).

The reactants were introduced in a total volume of 300 µL, in the following order: ultrapure water, alkali or acid, scavenger, spin-trap, activator, and H_2O_2. Unless otherwise stated, the following concentrations were respected: 5.6 M DMSO, approximately 5 M sodium formate, 6.0×10^{-2} M DMPO, 1.5×10^{-5} M $CuSO_4$, 3.0×10^{-5} M Phen, 1.0×10^{-4} M H_2O_2, and 6.0×10^{-2} M NaOH. For EPR experiments at 100 K, some trials were conducted with 10-fold Cu(II) and phenanthroline concentrations (1.5×10^{-4} M $CuSO_4$, 3.0×10^{-4} M Phen).

Under near-neutral conditions (no addition of NaOH), the pH was between 7.5 and 9 (7.5–7.6 in the presence of H_2O_2, around 8–8.6 in the absence of H_2O_2, and pH 9 when adding sodium formate). Under strong alkaline conditions (0.02 M NaOH), the pH was of 12.5. The use of scavengers induced some pH variations. With formate, the pH was around 9 in the absence of NaOH and was equal to 12.5 with NaOH. With DMSO, the pH was around 9 alone, around 8 with Cu-Phen, 7.6 with Cu-Phen + H_2O_2, and 14 with Cu–Phen + H_2O_2 + NaOH.

A "Fenton control" was performed for comparison with $FeSO_4$ replacing $CuSO_4$, at the same molar concentrations, and with the addition of H_2SO_4 to reach a pH of 3.

2.1.2. EPR Experiments

X-band EPR spectra were recorded with a Bruker EMX Plus spectrometer equipped with a standard ER4102ST Bruker cavity, either at room temperature or after heating. The instrument settings were the following: receiver gain 30 dB, modulation amplitude 1 G, and microwave power 0.02 mW. The tested samples were aqueous solutions of $CuSO_4$, Phen and Cu–Phen (called activators) with or without hydrogen peroxide, in the presence of DMPO as a spin-trap and DMSO or sodium formate as hydroxyl radical scavengers. After preparation, the solution was transferred to a bottom-sealed Pasteur pipette and

immediately analyzed. For the trials requiring heating, a heat gun was used to heat the pipette for approximately 15 s, after which the pipette was placed in the EPR cavity. All spectra in Section 3 display the same intensity scale. Note that a first measurement was made immediately and was repeated after 5 and/or 10 min to verify that the signal was quite stable. As it was, the presented spectra were considered representative of the system during the first 10 min.

Three complementary methods were used: simple spin-trapping (DMPO), spin-trapping after scavenging with DMSO (DMSO + DMPO), and after scavenging with $HCOO^-$ ($HCOO^-$ + DMPO).

Depending on the method and experimental conditions used to measure the rate constants in the literature, k(DMPO/$HO^\bullet$) ranges from 1.9×10^9 to 4.3×10^9 $M^{-1}s^{-1}$ [13,18,22].

The scavenging reactions of dimethyl sulfoxide and formate are the following:

$$(CH_3)_2SO + HO^\bullet \rightarrow CH_3SO(OH) + CH_3^\bullet \xrightarrow{DMPO} DMPO - CH_3^\bullet$$
$$(CH_3)_2SO + HO^\bullet \rightarrow CH_3SO(OH) + CH_3^\bullet \xrightarrow{DMPO} DMPO - CH_3^\bullet$$

where k(DMSO/$HO^\bullet$) = 4.2×10^9 to 7.1×10^9 $M^{-1}s^{-1}$ [23–25].

$$HCOO^- + HO^\bullet \rightarrow H_2O + COO^{\bullet -} \xrightarrow{DMPO} DMPO - COO^{\bullet -}$$

where k($HCOO^-$/$HO^\bullet$) = 2.5×10^9 to 2.9×10^9 $M^{-1}s^{-1}$ [18,26]. The rate constants of formic acid vary with pH: in neutral aqueous solution at room temperature, k(HCOOH/$HO^\bullet$) = 2.45×10^9 to 3.1×10^9 $M^{-1}s^{-1}$ [24]; at acidic pH, k(HCOOH/$HO^\bullet$) = 5×10^9 to 6.8×10^9 $M^{-1}s^{-1}$ [26].

Some EPR experiments were also carried out at 100 K to study copper complexation. The instrument settings were the following: receiver gain 30 dB, modulation amplitude 4 G, attenuation 10 dB. In this case, the samples were introduced in EPR quartz cells of 4 mm outer diameter and 0.5 mm wall thickness.

2.2. Result Analysis: Integration and Simulations

Most EPR simulations were conducted using the free isotropic simulation program SimEPR, provided by the (US) National Institute of Environmental Health Sciences' Public Electron Paramagnetic Resonance Software Tools [27,28]. It was useful to confirm the assignment of the experimental constants to the most probable radical species.

For the EPR experiments at 100 K, the Easyspin software [29] was used with graphical interface Simultispin [30].

Additional data regarding the simulation process and fitted spectra can be found in the Supplementary Materials.

3. Results and Discussion

The formation of $HO^\bullet$ was evaluated using the DMPO spin-trap, both in the absence of alkali and under strong alkaline conditions. The main results are gathered in Table 1a,b. The entry numbers will be used in the paper to refer to each experiment, e.g., DMPO + $CuSO_4$ is "exp 1".

Table 1: (**a**) Integration and simulation results at near-neutral pH: total peak area, and distribution of DMPO adducts and degradation products for some experiments, as relative areas of each radical, in percent. (**b**) Integration and simulation results at alkaline pH (with NaOH): total peak area, and distribution of DMPO adducts and degradation products for some experiments, as relative areas of each radical, in percent.

Entry	$HCOO^-$	DMSO	H_2O_2	Additive	Details	Total Peak Area (a.u.)	DMPO–OH (%)	DMPO–CH_3 (%)	DMPO–COO^- (%)	DMPO–R (%)	Triplet (%)
					(**a**)						
1				$CuSO_4$		1.12	5			74	8
2				Cu-Phen		1.46	6			77	17
3			x	Cu-Phen		1.29	38			54	8
4		x	x	Cu-Phen		1.2	18	73		4.5	4.5
5	x		x	Cu-Phen		0.65	18		49	28	5
6	x		x	Cu-Phen	+10′ [b]	0.54	14		70	12	4
7	x		x	Cu-Phen	H [a]	0.79	10		79	8	3
8			x	$CuSO_4$		0.89	7			57	16
9		x	x	$CuSO_4$		0.83	16			76	8
10	x		x	$CuSO_4$		0.21	15		23	34	10
11			x	$FeSO_4$	pH 3	0.43	86			7	7
12		x		$CuSO_4$		0.82	14			78	8
13		x		Cu-Phen		1.0	22			72	6
14	x			Cu-Phen		0.79	19		11	58	12
15	x			Cu-Phen	H	0.84	11		72	13	4
16			x	/	H	0.35	38			38	24
					(**b**)						
17				$CuSO_4$		0.62	2			72	6
18				Cu-Phen		0.55	17			58	10
19	x			Cu-Phen	+8′ [c]	0.54			92	8	
20			x	Cu-Phen		0.72	21			69	11
21		x	x	Cu-Phen		0.12	16	80			5
22	x		x	Cu-Phen		0.72	17		47	28	8

For all controls conducted in the absence of DMPO, no EPR signal was observed (not shown). In some cases (entries 1, 8, and 10), secondary adducts were found by simulation. Their relative areas (%) are presented in the Supplementary Materials. [a] Heating. [b] +10 min. For all controls conducted in the absence of DMPO, no EPR signal was observed (not shown). In some cases (entries 17 and 18), secondary adducts were found by simulation. Their relative areas (%) are presented in the Supplementary Materials. [c] +8 min.

3.1. Results at Near-Neutral pH

Before investigating the decomposition of H_2O_2 by Cu–Phen, the stability of DMPO in the presence of Cu–Phen (exp 2) was evaluated (Figure 3). In the presence of DMPO, the EPR spectrum of a solution of Cu–Phen displays features corresponding to three different radical adducts: DMPO–OH, DMPO–R, and a radical showing triplet splitting lines (Figure 3a). The addition of DMSO (exp 13) does not reduce the DMPO–OH signal, indicating that DMPO–OH does not originate from the trapping of $HO^{\bullet}$, but from nucleophilic addition of water. This was confirmed using the other radical scavenger, $HCOO^-$ (exp 14), as illustrated in Figure S6. Note that the hyperfine splitting constants for DMPO–OH in the presence of DMSO (and water) are different from those in water only, as described in the literature [31,32].

The DMPO–R and the species that shows triplet splitting lines (we will name it "triplet radical" in figure legends for easier reading) are most likely due to the decomposition of DMPO in the presence of copper. Controls have been carried out to understand the origin of these species. While DMPO does not exhibit any signal in the absence or presence of phenanthroline, an EPR signal is observed in the presence of $CuSO_4$ (exp 1), similar to that of DMPO + Cu–Phen, but less intense (about 50%; see Table 1a entries 1 and 2 and Figure 3b). The higher intensity of the DMPO-R and triplet signals observed with Cu–Phen compared to $CuSO_4$ demonstrates that DMPO is degraded faster in the presence of Cu–Phen. This is consistent with the redox potential of $Cu^{II}(Phen)_2/Cu^{I}(Phen)_2$ that is slightly higher than that of Cu^{II}/Cu^{I} (0.17 and 0.16 V, respectively) [15].

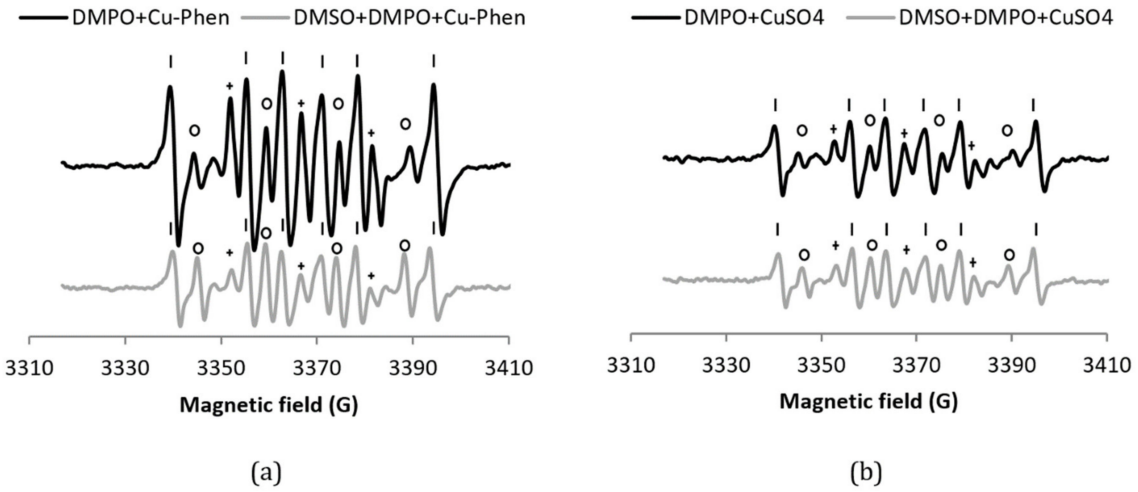

Figure 3. X-band EPR spectra of (**a**) DMPO + Cu–Phen and DMSO + DMPO + Cu–Phen; (**b**) DMPO + $CuSO_4$ and DMSO + DMPO + $CuSO_4$.The simulations revealed the presence of at least three radical species in each case. With DMPO + Cu–Phen (exp 2): DMPO–OH, a_N = 15.088 G, a_H = 14.943 G; DMPO–R, a_N = 15.781 G, a_H = 23.27 G; "triplet radical", a_N = 14.354 G. With DMSO + DMPO + Cu–Phen (exp 13): DMPO–OH, a_N = 14.697 G, a_H = 13.82 G; DMPO–R, a_N = 15.488 G, a_H = 22.635 G; "triplet radical", a_N = 14.305 G. With DMPO + $CuSO_4$ (exp 1); DMPO–OH, a_N = 15.798 G, a_H = 14.928 G [33,34]; DMPO–R, a_N = 15.798 G, a_H = 23.237 G [35]; "triplet radical", a_N = 14.609 G; other, a_N = 16.323 G, a_H = 26.653 G (uncertain). With DMSO + DMPO + $CuSO_4$ (exp 12): DMPO–OH, a_N = 14.697 G, a_H = 14.015 G; DMPO–R, a_N = 15.439 G, a_H = 22.586 G; "triplet radical", a_N = 14.354 G; Assignments: o = DMPO–OH, | = DMPO–R, + = "triplet radical".

In the present work, the coordination of DMPO to the Cu(II) ion was evidenced by EPR spectra recorded at 100 K with DMPO 60 mM and Cu(II) 0.15 mM (Figure 4). Under such conditions (low temperature and Cu(II) concentration 10 times larger than in the spin-trapping experiments), the EPR signal corresponding to the Cu(II) ion ($S = 1/2$, d^9) is observed with a typical axial spectrum characterized by a quartet in the parallel component arising from hyperfine interaction ($I_{Cu} = 3/2$).

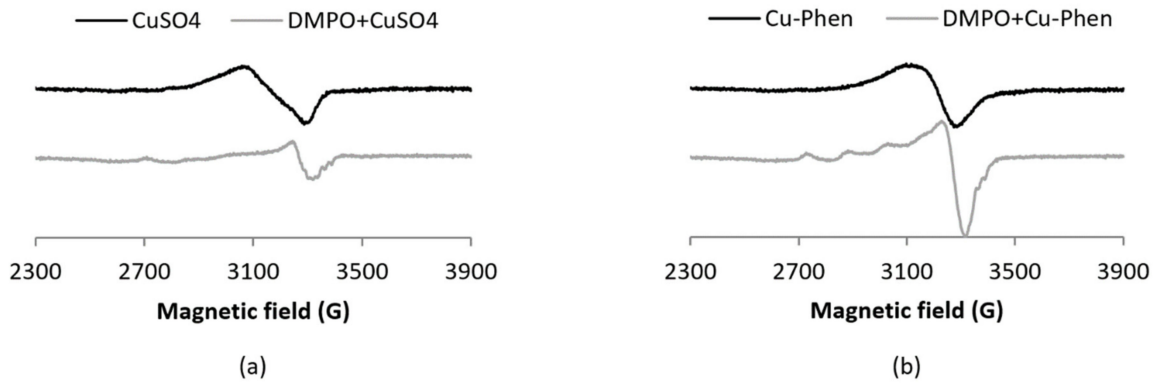

Figure 4. X-band EPR spectra at 100 K of (**a**) $CuSO_4$ with and without DMPO and (**b**) Cu–Phen with and without DMPO, [Cu] = 0.15 mM, [DMPO] = 60 mM. For a solution of copper with an equimolar amount of DMPO, i.e., 0.15 mM, the structuration is no longer visible (results not shown), indicating a low affinity of DMPO for copper.

The addition of DMPO notably modifies the EPR spectra of both Cu–Phen and $CuSO_4$, as demonstrated by changes in the g-value anisotropy. Such changes evidence the difference in coordination geometry around the Cu ion. The present work also highlights the fact that Phen remains bound to Cu when DMPO and Cu–Phen are mixed, since the spectra of Cu–DMPO adducts with or without Phen display different EPR parameters (see Table S24 in the Supplementary Materials). Besides, the absence of a decrease of the signal integration when DMPO is added demonstrates that Cu(II) is not reduced by DMPO into Cu(I) under these experimental conditions.

The H_2O_2/Cu–Phen system (exp 3) was tested in the presence of DMPO (Figure 5), leading to an intense DMPO–OH spectrum, a multiplet assigned to DMPO–R, and a triplet splitting. The simulations confirm that the DMPO–R and the radical that shows triplet splitting lines are the same as without H_2O_2. The DMPO–OH signal is 4.8 times more intense than with Cu–Phen alone (38% DMPO–OH for a total area of 1.29 (entry 3 in Table 1) vs. 7% for a total area of 1.46 (entry 2)). This already indicates that hydroxyl radicals are the major species responsible for the formation of DMPO–OH with H_2O_2/Cu–Phen. Note that no hydroxyl radicals are present at room temperature with hydrogen peroxide alone.

In the presence of DMSO (exp 4, see Figure 5 and entry 4 in Table 1a), a drop of the DMPO–OH signal is accompanied with the detection of a new carbon-centered DMPO adduct, assigned to DMPO–CH_3 based on its EPR parameters [33,36]. DMPO–CH_3 is highly predominant, representing 73% of the detected radicals. This was confirmed when sodium formate was used as scavenger (exp 5, Figure S9), with 49% of DMPO–COO^- among the detected radicals (entry 5 in Table 1a).

These experiments demonstrate that hydroxyl radicals are produced in aqueous solution in the presence of both H_2O_2 and Cu–Phen. The apparent disappearance of the DMPO–OH signal in the presence of both radical scavengers is consistent with the absence of nucleophilic water addition in this case. This can be explained by the low constant rate of the DMPO/H_2O reaction, or by the fact that copper activates H_2O_2's decomposition rather than induces nucleophilic addition of water onto DMPO. When analyzing the solution after 10 min at room temperature (Figure S10), the DMPO–COO^- signal is more intense than after direct acquisition, meaning that the system is still active after a few minutes.

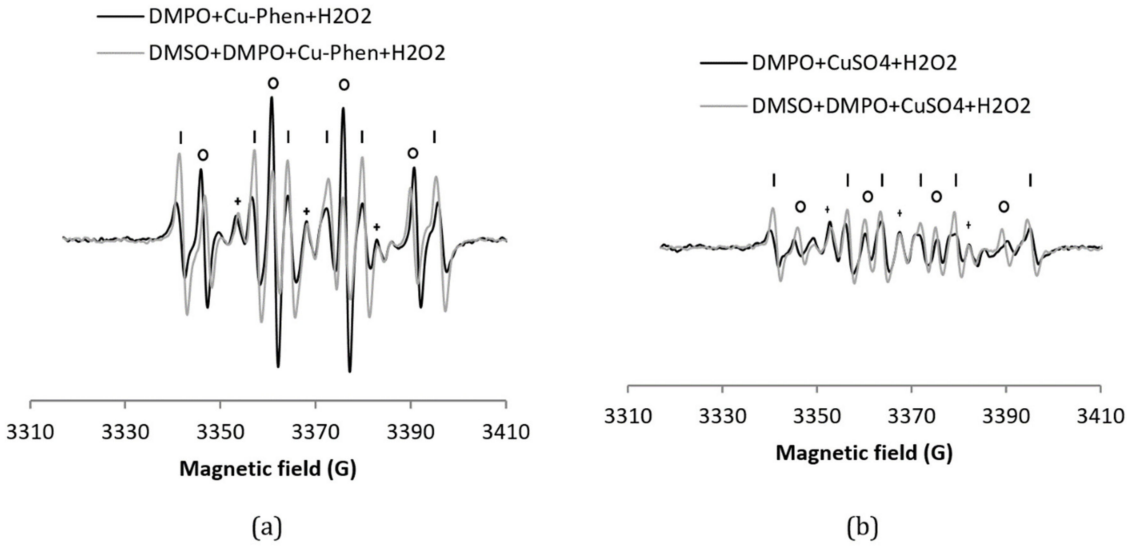

Figure 5. X-band EPR spectra of (**a**) DMPO + Cu–Phen + H_2O_2 and DMSO + DMPO + Cu–Phen + H_2O_2; (**b**) DMPO + $CuSO_4$ + H_2O_2 and DMSO + DMPO + $CuSO_4$ + H_2O_2. The simulations revealed the presence of three to five radical species in each case. With DMPO + Cu–Phen + H_2O_2 (exp3); DMPO–OH, a_N = 15.0 G, a_H = 14.805 G; DMPO–R, a_N = 15.781 G, a_H = 23.342 G; "triplet radical", a_N = 14.549 G; with DMSO + DMPO + Cu–Phen + H_2O_2 (exp 4): DMPO–OH, a_N = 14.7 G, a_H = 13.851 G; DMPO–R, a_N = 15.7 G, a_H = 22.651 G; "triplet radical", a_N = 14.349 G; other, a_N = 15.786 G, a_H = 20.11 G (minor and uncertain). With DMPO + $CuSO_4$ + H_2O_2 (exp 8): DMPO–OH, a_N = 15.244 G, a_H = 14.83 G; DMPO–R, a_N = 15.70 G, a_H = 23.51 G; "triplet radical", a_N = 14.598 G; other, a_N = 13.975 G, a_H = 21.435 G (minor and uncertain); other, a_N = 12.195 G, a_H = 11.463 G (3 H, also minor and uncertain); with DMSO + DMPO + $CuSO_4$ + H_2O_2 (exp 9): DMPO–OH, a_N = 14.707 G, a_H = 13.951G; DMPO–R, a_N = 15.651 G, a_H = 22.658 G; "triplet radical", a_N = 14.354 G - Assignments: o = DMPO–OH, | = DMPO–R, + = "triplet radical".

For comparison, the $H_2O_2/CuSO_4$ system (exp 8, Figure 5b) does not exhibit much difference with $CuSO_4$ alone (only an increase of 7.5% of DMPO–OH) (entry 8 in Table 1a). The DMPO–OH signal is very weak compared to that observed earlier with H_2O_2/Cu–Phen. Since DMSO does not seem to scavenge hydroxyl radicals (exp 9), sodium formate was also tested (exp 5, Figure 6). In its presence, the DMPO–OH signal almost disappears with the concomitant appearance of the signal typical of DMPO–COO^-. This shows that only a low amount of hydroxyl radicals is generated under such conditions. Consistently, the group of Bhattacharjee [37] also observed DMPO–OH at physiological pH with DMPO, H_2O_2, and $CuCl_2$. However, they did not identify the origin of the DMPO–OH adduct because they did not use a radical scavenger.

As illustrated in Figure 6, the DMPO–COO^- signal with H_2O_2 + Cu-Phen is more intense than with H_2O_2 + $CuSO_4$, approximately 85% higher (total area of 0.65 including 49% DMPO–COO^- vs. 0.21 including 23% DMPO–COO^-, see entries 5 and 10 respectively in Table 1a). This unambiguously confirms the stronger H_2O_2 decomposition in the presence of Cu–Phen. Similarly, in the context of dye decolorization, Nerud et al. [38] observed that H_2O_2/Cu^{II}–pyridine was more effective than H_2O_2/Cu^{II} at pH 3 to 9. The authors proposed that hydroxyl radicals were probably involved in the decolorization, since $HO^\bullet$ scavengers such as superoxide dismutase inhibited the color-stripping.

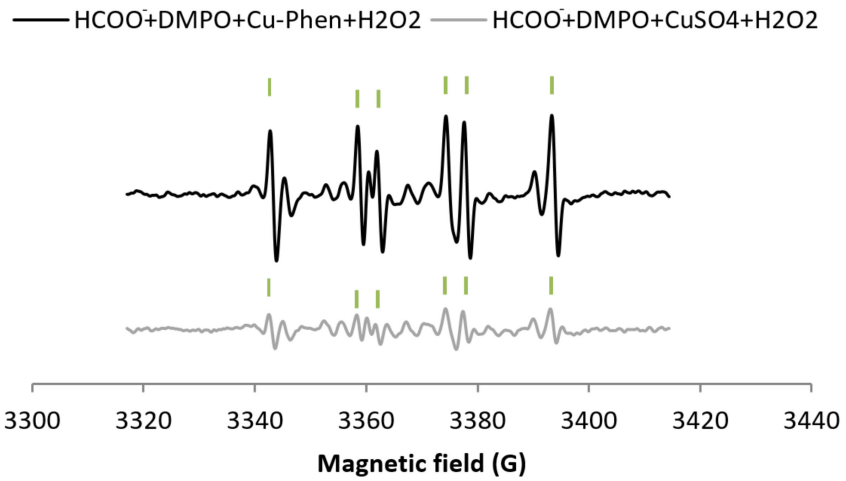

Figure 6. Comparison between the X-band EPR spectra of $HCOO^-$ + DMPO + Cu–Phen + H_2O_2 (exp 5) and $HCOO^-$ + DMPO + $CuSO_4$ + H_2O_2 (exp 10) - Assignments: | = DMPO–COO^-.

Since H_2O_2/Cu–Phen is the most efficient system to produce hydroxyl radicals, its efficiency was compared to a reference system: the Fenton reagent. $FeSO_4$ was thus used instead of Cu–Phen, under strong acidic conditions, with the same H_2O_2 and metal concentrations (exp 11, Figure 7).

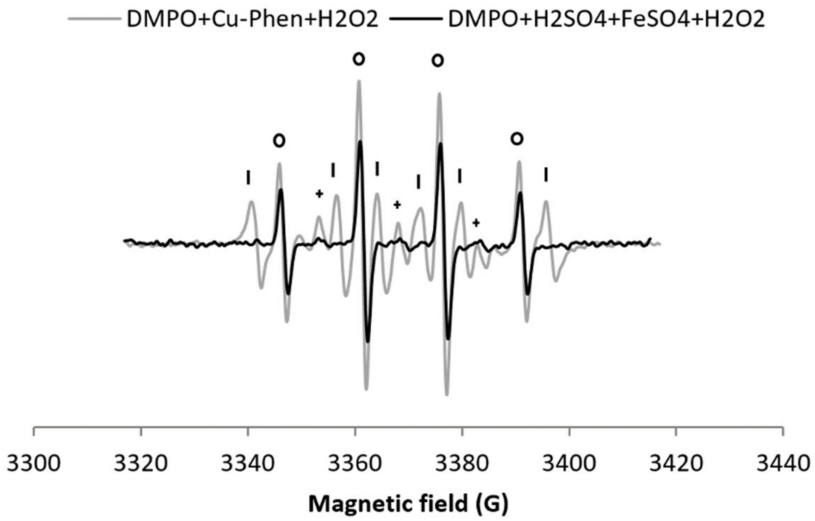

Figure 7. X-band EPR spectrum of DMPO + Cu–Phen + H_2O_2 at near-neutral pH compared to DMPO + $FeSO_4$ + H_2O_2 at pH 3 (same concentrations of H_2O_2 and [Fe] = [Cu]). With DMPO + $FeSO_4$ + H_2O_2 at pH 3 (exp 11), the simulation revealed the presence of three radical species: DMPO–OH, a_N = 15.00 G, a_H = 14.732 G; DMPO–R, a_N = 14.675 G, a_H = 21.703 G; "triplet radical", a_N = 14.793 G - Assignments: o = DMPO–OH, | = DMPO-R, + = "triplet radical".

As expected, the Fenton control gives a clear four-line signal typical of DMPO–OH (entry 11 in Table 1a). Yet, it is 25% less intense than for H_2O_2/Cu–Phen (total area of 0.43 including 86% DMPO–OH found with H_2O_2/Fe, compared to 1.29 including 38% DMPO–OH with H_2O_2/Cu-Phen). Assuming that nucleophilic addition of water does not occur neither in the Fenton system nor in the H_2O_2/Cu–Phen system (as discussed earlier), the H_2O_2/Cu–Phen system is thus a little more active than the Fenton reactant under similar conditions. Still, the $HO^\bullet$ generation of H_2O_2/Cu–Phen is in the same range as that of the Fenton system.

3.2. Results at Alkaline pH

At alkaline pH, DMPO is degraded faster than at near-neutral pH, both alone and with phenanthroline (same intensity, see Figure S11), and the three-line signal attesting the DMPO degradation is observed even in the absence of copper or hydrogen peroxide. This is consistent with easier nucleophilic addition at alkaline pH.

With $CuSO_4$ (exp 17), the signal exhibits mostly DMPO degradation products, whereas with Cu–Phen (exp 18), the DMPO–OH signal can be clearly observed (Figure S12). Therefore, the Cu–Phen solution (the main species being $CuPhen(OH)_2$ in this case) was analyzed in the presence of the sodium formate scavenger (exp 19, Figure S13), leading to the generation of the typical DMPO–COO^- signal, and thus confirming that hydroxyl radicals are generated under such conditions. The generation of $HO^\bullet$ in the absence of hydrogen peroxide can be rationalized by the catalytic reduction of soluble oxygen by Cu–Phen under alkaline conditions [39–41].

As previously examined under near-neutral conditions, the influence of DMPO on the electronic structure of the Cu^{II} ion was tested at alkaline pH. The difference in the 100 K-EPR spectra of Cu–Phen recorded at both pHs (see Figures S19 and S23) is consistent with the binding of a hydroxo ligand at the Cu site [36]. When DMPO is added, a new EPR spectrum with well-resolved hyperfine couplings is observed, distinct from that obtained with $CuSO_4$ at alkaline pH. This agrees with the fact that DMPO can coordinate copper at both alkaline and near-neutral pHs (Figure 8).

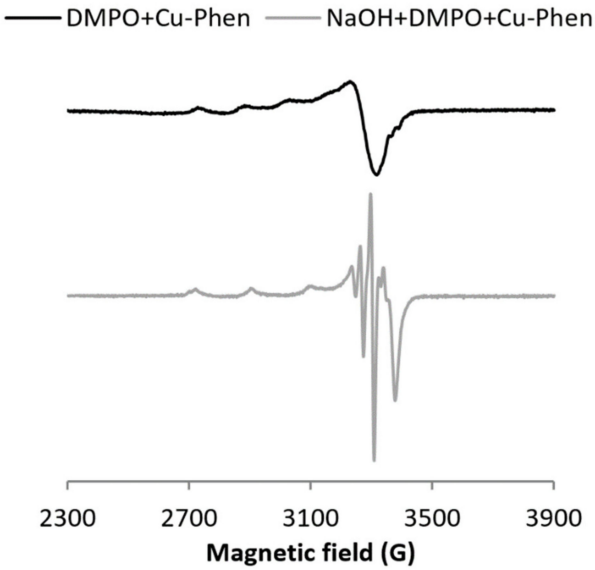

Figure 8. X-band EPR spectra at 100 K of DMPO + Cu–Phen with and without NaOH-[Cu] = 0.15 mM, [DMPO] = 60 mM.

When H_2O_2 is added to the Cu–Phen system (exp 20), a DMPO-OH signal appears (Figure 9). $HO^\bullet$ scavenging with DMSO (exp 21) leads to the disappearance of the DMPO–OH signal and the apparition of DMPO–CH_3, thus confirming that the DMPO–OH signal is only due to the presence of hydroxyl radicals (Figure 9a). As a confirmation, the formation of DMPO–COO^- is observed in the presence of sodium formate (exp 22, Figure 9b). However, the generation of $HO^\bullet$ is less intense (Figure 10) and slower (Figure S15) than at lower pH. Note that as observed at near-neutral pH, the hydroxyl radical is not produced in the alkaline $H_2O_2/CuSO_4$ system (Figure S16).

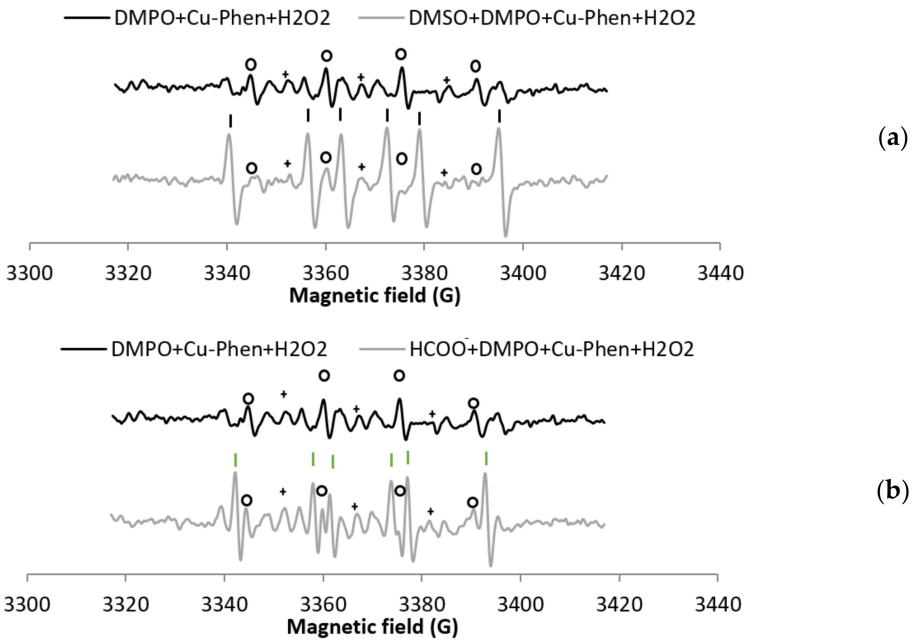

Figure 9. X-band EPR spectra of (**a**) NaOH + DMPO + Cu–Phen + H_2O_2 and NaOH + DMSO + DMPO + Cu–Phen + H_2O_2 and (**b**) NaOH + DMPO + Cu–Phen + H_2O_2 and NaOH + $HCOO^-$ + DMPO + Cu–Phen + H_2O_2-. The simulations revealed the presence of several radical species. Without scavenger (exp 20): DMPO–OH, a_N = 15.439 G, a_H = 15.049 G; DMPO–R, a_N = 15.79 G, a_H = 23.488 G; "triplet radical", a_N = 14.646 G. With DMSO (exp 21): DMPO–OH, a_N = 13.926 G, a_H = 14.072 G; DMPO–CH_3, a_N = 15.937 G, a_H = 22.658 G; "triplet radical", a_N = 14.788. With $HCOO^-$ (exp 22): DMPO–OH, a_N = 15.342 G, a_H = 15.537 G; DMPO–R, a_N = 15.742 G, a_H = 24.123 G (minor); "triplet radical", a_N = 14.691 G; DMPO–COO^-, a_N = 15.805 G, a_H = 19.049 G - Assignments: o = DMPO–OH, | = DMPO–CH_3, + = "triplet radical", | = DMPO–COO^-.

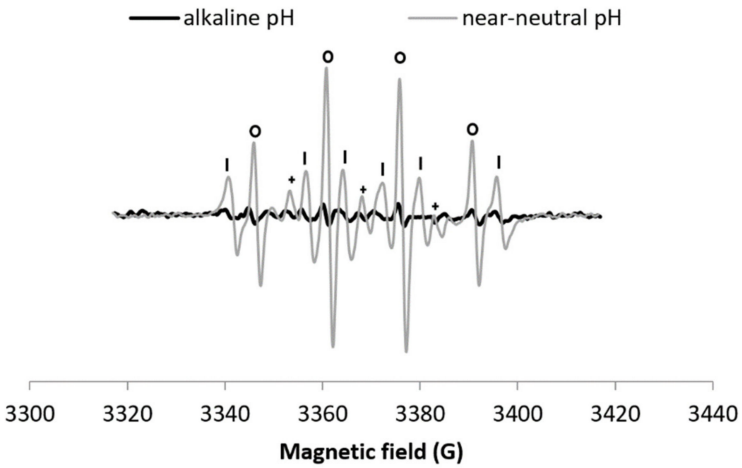

Figure 10. X-band EPR spectra of NaOH + DMPO + Cu–Phen + H_2O_2 (exp 20) and DMPO + Cu–Phen + H_2O_2 (exp 3). Comparison between alkaline and near-neutral pH - Assignments: o = DMPO–OH, | = DMPO–R, + = "triplet radical".

4. Concluding Remarks

Under near-neutral and alkaline conditions, DMPO was shown to be degraded in the presence of copper ($CuSO_4$ and Cu–Phen), but not with phenanthroline alone. Indeed, nucleophilic addition of water onto DMPO was evidenced, leading to the formation of the DMPO–OH adduct in the absence of hydroxyl radicals. To identify the origin of the observed DMPO–OH, two $HO^\bullet$ scavengers (sodium formate and DMSO) have been

compared, and their efficiency is pH dependent. While sodium formate was found to be the best scavenger at near neutral pH, under alkaline conditions, both scavengers display similar activity. Besides, we have shown that DMPO coordinates the copper(II) ion under both conditions in the presence or absence of Phen.

The addition of Cu–Phen into a hydrogen peroxide solution at near-neutral pH and alkaline pH was proven to cause its decomposition into hydroxyl radicals. Interestingly, at near-neutral pH, the Cu–Phen system demonstrates an efficiency similar to that of the Fenton system at acidic pH, while $CuSO_4$ displays only a poor production of hydroxyl radicals. This evidences the role of the Phen ligand.

The presence of Phen influences both the electronic structure of the copper(II) complexes and their structural properties. Accordingly, Burkitt et al. [15] showed that at neutral pH, the redox potential of $Cu^{II}(Phen)_2/Cu^{I}(Phen)_2$ is slightly higher than that of Cu^{II}/Cu^{I} (0.17 and 0.16 V, respectively), consistently with higher degradation of DMPO in the presence of Phen.

Besides, at alkaline pH, the Cu–Phen speciation is different from near-neutral pH [42]. At high pH, two hydroxo ligands are coordinated to the copper(II) ion to mainly form $CuPhen(OH)_2$, while at near-neutral pH, $Cu(Phen)_2$ is the major species. Such difference in coordination would explain a weaker and slower hydroxyl radical generation at alkaline pH.

Supplementary Materials: The following are available online at https://www.mdpi.com/2076-3417/11/2/687/s1, Figure S1. Typical DMPO–CH3 signal [15] (a) and DMPO–COO- signal (simulated based on constants given by Mossoba et al. [26]) (b)-DMPO–CH3: aH = 16.1 G, aN = 23.0 G; DMPO–COO-: aH = 15.6 G, aN = 18.7 G, Table S1. DMPO + Cu–Phen–Simulation results, Figure S2. Comparison between the experimental and simulated spectra of DMPO + Cu–Phen, Table S2. DMPO + Cu–Phen + H2O2—simulation results, Figure S3. Comparison between the experimental and simulated spectra of DMPO + Cu–Phen + H2O2 at near-neutral pH, Table S3. DMSO + DMPO + Cu–Phen + H2O2–simulation results, Figure S4. Comparison between the experimental and simulated spectra of DMSO + DMPO + Cu–Phen + H2O2, Table S4. HCOO- + DMPO + Cu–Phen + H2O2–simulation results, Figure S5. Comparison between the experimental and simulated spectra of HCOO- + DMPO + Cu–Phen + H2O2, Table S5. DMPO + CuSO4–simulation results, Table S6. HCOO- + DMPO + Cu–Phen + H2O2 t = 5 min–Simulation results, Table S7. HCOO- + DMPO + Cu–Phen + H2O2 after heating–simulation results, Table S8. DMPO + CuSO4 + H2O2–simulation results, Table S9. DMSO + DMPO + CuSO4 + H2O2–simulation results, Table S10. HCOO- + DMPO + CuSO4 + H2O2–simulation results, Table S11. DMPO + FeSO4 + H2O2 at pH 3–simulation results, Table S12. DMSO + DMPO + CuSO4–simulation results, Table S13. DMSO + DMPO + Cu–Phen–simulation results, Table S14. HCOO- + DMPO + Cu–Phen–simulation results, Table S15. HCOO- + DMPO + Cu–Phen after heating–simulation results, Table S16. DMPO + H2O2 after heating–simulation results, Table S17. NaOH + DMPO + CuSO4–simulation results, Table S18. NaOH + DMPO + Cu–Phen–simulation results, Table S19. NaOH + HCOO- + DMPO + Cu–Phen t = 8 min–simulation results, Table S20. NaOH + DMPO + Cu-Phen + H2O2–simulation results, Table S21. NaOH + DMSO + DMPO + Cu-Phen + H2O2–simulation results, Table S22. NaOH + HCOO- + DMPO + Cu-Phen + H2O2–simulation results, Figure S6. X-band EPR spectra of DMPO + Cu–Phen and HCOO- + DMPO + Cu–Phen-the simulation revealed the presence of four radical species with HCOO- + DMPO + Cu–Phen: DMPO–OH, aN = 14.843 G, aH = 15.428 G; DMPO–R, aN = 15.644 G, aH = 23.244 G; triplet, aN = 14.593 G; DMPO–COO-, aN = 15.683 G, aH = 19.293 G-Assignments: o = DMPO-OH, | = DMPO-R, + = triplet, ǀ = DMPO-COO-, Figure S7. X-band EPR spectra of DMPO + Cu–Phen and HCOO- + DMPO + Cu–Phen after heating—the simulation revealed the presence of four radical species with HCOO- + DMPO + Cu–Phen: DMPO–OH, aN = 14.746 G, aH = 15.428 G; DMPO-R, aN = 15.644 G, aH = 23.342 G; triplet, aN = 14.788 G; DMPO–COO-, aN = 15.781 G, aH = 19.0 G-Assignments: o = DMPO–OH, | = DMPO–R, + = triplet, ǀ = DMPO–COO-, Figure S8. X-band EPR spectra of DMPO + H2O2 at ambient temperature and after heating. The simulation revealed the presence of three radical species after heating: DMPO–OH, aN = 14.756 G, aH = 15.391 G; DMPO–R, aN = 14.813 G, aH = 21.535 G; triplet, aN = 14.842 G-Assignments: o = DMPO–OH, | = DMPO–R, + = triplet, Figure S9. X-band EPR spectra of DMPO + Cu–Phen + H2O2 and HCOO- + DMPO + Cu–Phen + H2O2-With HCOO-, the simulation revealed the presence of four radical species DMPO–OH,

aN = 14.902 G, aH = 15.233 G; DMPO–R, aN = 15.64 G, aH = 23.266 G; triplet, aN = 14.593 G; DMPO–COO-, aN = 15.749 G, aH = 19.098 G-Assignments: o = DMPO–OH, | = DMPO–R, + = triplet, ǀ = DMPO–COO-, Figure S10. X-band EPR spectra of HCOO- + DMPO + Cu–Phen + H2O2 at ambient temperature at t = 0 and t = 10 min and after heating—the simulations revealed the presence of four radical species. At t = 10 min: DMPO–OH, aN = 15.049 G, aH = 14.976 G; DMPO–R, aN = 15.651 G, aH = 23.872 G; triplet, aN = 14.463 G; DMPO–COO-, aN = 15.781 G, aH = 19.098 G [26], [32]. After heating: DMPO–OH, aN = 15.0 G, aH = 15.074G; DMPO–R, aN = 15.602 G, aH = 23.607 G; triplet, aN = 14.512 G; DMPO–COO-, aN = 15.781 G, aH = 19.049 G-Assignments: ǀ = DMPO–COO-, Figure S11. X-band EPR spectra of NaOH + DMPO and NaOH + DMPO + Phen-Assignments: + = triplet, Figure S12. X-band EPR spectra of NaOH + DMPO + CuSO4 and NaOH + DMPO + Cu–Phen—the simulations revealed the presence of four radical species in both solutions. With CuSO4: DMPO–OH, aN = 15.195 G, aH = 15.294 G; DMPO–R, aN = 15.741 G, aH = 23.488 G; triplet, aN = 14.549 G; other, aH = 17.975 G (2 H, uncertain). With Cu-Phen: DMPO–OH, aN = 15.234 G, aH = 15.623 G; DMPO–R, aN = 15.742 G, aH = 23.83 G; triplet, aN = 14.398 G; other, aN = 14.999 G, aH = 21.246 G-Assignments: o = DMPO–OH, | = DMPO–R, + = triplet, Figure S13. X-band EPR spectra of NaOH + HCOO- + DMPO + Cu–Phen at t = 0, t = 5 min and t = 8 min—the simulations revealed the presence of two radical species: DMPO–R, aN = 15.595 G, aH = 22.756 G; DMPO–COO-, aN = 15.805 G, aH = 19.00 G, Figure S14. X-band EPR spectra at 100 K of (a) NaOH + Cu–Phen with and without DMPO–[Cu] = 0.15 mM, [DMPO] = 60 mM, and (b) NaOH + CuSO4 with and without DMPO–[DMPO] = 60 mM. The addition of DMPO at the same concentration as Cu–Phen (0.15 mM) did not seem to modify the structure of Cu(II) (not shown), Figure S15. X-band EPR spectra of NaOH + DMPO + Cu–Phen + H2O2 at t = 0 and at t = 5 min-Assignments: o = DMPO–OH, Figure S16. X-band EPR spectra of NaOH + DMPO + CuSO4 and NaOH + DMPO + CuSO4 + H2O2, Table S23. EPR hyperfine coupling constants of the observed radical species: experimental and reference values (see Buettner's spin adduct parameter tables [13]) for comparison, Table S24. Simulation results for the EPR spectra recorded at 100 K: EPR parameters given as g-values and A-values for each experimental spectrum, Figure S17. X-band EPR spectrum at 100 K of CuSO4 and corresponding simulated spectrum, Figure S18. X-band EPR spectrum at 100 K of DMPO + CuSO4 and corresponding simulated spectrum, Figure S19. X-band EPR spectrum at 100 K of Cu–Phen and corresponding simulated spectrum, Figure S20. X-band EPR spectrum at 100 K of DMPO + Cu–Phen and corresponding simulated spectrum, Figure S21. X-band EPR spectrum at 100 K of NaOH + CuSO4 and corresponding simulated spectrum, Figure S22. X-band EPR spectrum at 100 K of NaOH + DMPO + CuSO4 and corresponding simulated spectrum, Figure S23. X-band EPR spectrum at 100 K of NaOH + Cu–Phen and corresponding simulated spectrum, Figure S24. X-band EPR spectrum at 100 K of NaOH + DMPO + Cu–Phen and corresponding simulated spectrum.

Author Contributions: This study was supervised by N.M. and G.M. Formal analysis and investigation were performed by E.W., with the help of F.M. who ran the spectroscopic measurements and software. E.W. wrote the original draft with the guidance of C.D., and F.M. and C.D. participated to review and editing. All authors have read and agreed to the published version of the manuscript.

Funding: This research received no external funding.

Institutional Review Board Statement: Not applicable.

Informed Consent Statement: Not applicable.

Data Availability Statement: The data presented in this study is available in the article and supplementary material.

Acknowledgments: LGP2 is part of the LabEx Tec 21 (Investissements d'Avenir-grant agreement n°ANR-11-LABX-0030) and of PolyNat Carnot Institute (Investissements d'Avenir-grant agreement n°ANR-16-CARN-0025-01). This research was made possible thanks to the facilities of the TekLiCell platform funded by the Région Rhône-Alpes (ERDF: European regional development fund) and to the EPR facilities of CNRS's research infrastructure RENARD (IR-RPE CNRS 3443).

Conflicts of Interest: The authors declare no conflict of interest. The funders had no role in the design of the study; in the collection, analyses, or interpretation of data; in the writing of the manuscript, or in the decision to publish the results.

References

1. Sigman, D.S.; Graham, D.R.; D'Aurora, V.; Stern, A.M. Oxygen-dependent cleavage of DNA by the 1,10-phenanthroline cuprous complex. Inhibition of Escherichia coli DNA polymerase I. *J. Biol. Chem.* **1979**, *254*, 12269–12272. [CrossRef]
2. Sigman, D.S. Nuclease activity of 1,10-phenanthroline-copper ion. *Acc. Chem. Res.* **1986**, *19*, 180–186. [CrossRef]
3. Thederahn, T.B.; Kuwabara, M.D.; Larsen, T.A.; Sigman, D.S. Nuclease activity of 1,10-phenanthroline-copper: Kinetic mechanism. *J. Am. Chem. Soc.* **1989**, *111*, 4941–4946. [CrossRef]
4. Oyoshi, T.; Sugiyama, H. Mechanism of DNA Strand Scission Induced by (1,10-Phenanthroline)copper Complex: Major Direct DNA Cleavage Is Not through 1′,2′-Dehydronucleotide Intermediate nor β-Elimination of Forming Ribonolactone. *J. Am. Chem. Soc.* **2000**, *122*, 6313–6314. [CrossRef]
5. Chikira, M.; Tomizawa, Y.; Fukita, D.; Sugizaki, T.; Sugawara, N.; Yamazaki, T.; Sasano, A.; Shindo, H.; Palaniandavar, M.; Antholine, W.E. DNA-fiber EPR study of the orientation of Cu(II) complexes of 1,10-phenanthroline and its derivatives bound to DNA: Mono(phenanthroline)-copper(II) and its ternary complexes with amino acids. *J. Inorg. Biochem.* **2002**, *89*, 163–173. [CrossRef]
6. Lu, L.-P.; Zhu, M.-L.; Yang, P. Crystal structure and nuclease activity of mono(1,10-phenanthroline) copper complex. *J. Inorg. Biochem.* **2003**, *95*, 31–36. [CrossRef]
7. Liu, C.; Zhou, J.; Li, Q.; Wang, L.; Liao, Z.; Xu, H. DNA damage by copper(II) complexes: Coordination-structural dependence of reactivities. *J. Inorg. Biochem.* **1999**, *75*, 233–240. [CrossRef]
8. Sigman, D.S.; Mazumder, A.; Perrin, D.M. Chemical nucleases. *Chem. Rev.* **1993**, *93*, 2295–2316. [CrossRef]
9. Simunkova, M.; Lauro, P.; Jomova, K.; Hudecova, L.; Danko, M.; Alwasel, S.; Alhazza, I.M.; Rajcaniova, S.; Kozovska, Z.; Kucerova, L.; et al. Redox-cycling and intercalating properties of novel mixed copper(II) complexes with non-steroidal anti-inflammatory drugs tolfenamic, mefenamic and flufenamic acids and phenanthroline functionality: Structure, SOD-mimetic activity, interaction with albumin, DNA damage study and anticancer activity. *J. Inorg. Biochem.* **2019**, *194*, 97–113. [CrossRef] [PubMed]
10. Das, S.; Lachenal, D.; Marlin, N. Production of pure cellulose from Kraft pulp by a totally chlorine-free process using catalyzed hydrogen peroxide. *Ind. Crop. Prod.* **2013**, *49*, 844–850. [CrossRef]
11. Halma, M.; Lachenal, D.; Marlin, N.; Deronzier, A.; Brochier, M.C.; Zarubin, M. H_2O_2 oxidation of lignin model dimers catalyzed by copper(II)– phenanthroline. *Ind. Crop. Prod.* **2015**, *74*, 514–522. [CrossRef]
12. Walger, E.; Rivollier, C.; Marlin, N.; Mortha, G. Activated hydrogen peroxide decolorization of a model azo dye-colored pulp. *Holzforschung* **2015**, *69*, 677–683. [CrossRef]
13. Hanna, P.M.; Mason, R.P. Direct evidence for inhibition of free radical formation from Cu(I) and hydrogen peroxide by glutathione and other potential ligands using the EPR spin-trapping technique. *Arch. Biochem. Biophys.* **1992**, *295*, 205–213. [CrossRef]
14. Buettner, G.R. Spin Trapping: ESR parameters of spin adducts 1474 1528V. *Free Radic. Biol. Med.* **1987**, *3*, 259–303. [CrossRef]
15. Burkitt, M.J.; Ying Tsang, S.; Ching Tam, S.; Bremner, I. Generation of 5,5-Dimethyl-1-pyrroline N-Oxide Hydroxyl and Scavenger Radical Adducts from Copper/H_2O_2 Mixtures: Effects of Metal Ion Chelation and the Search for High-Valent Metal–Oxygen Intermediates. *Arch. Biochem. Biophys.* **1995**, *323*, 63–70. [CrossRef]
16. Finkelstein, E.; Rosen, G.M.; Rauckman, E.J. Spin trapping of superoxide and hydroxyl radical: Practical aspects. *Arch. Biochem. Biophys.* **1980**, *200*, 1–16. [CrossRef]
17. Lauricella, R.; Tuccio, B. Détection et caractérisation de radicaux libres après piégeage de spins. In *La Spectroscopie de Résonance Paramagnétique Électronique: Applications*; EDP Sciences: Les Ulis, France, 2014; pp. 49–78. ISBN 978-2-7598-1292-9.
18. Eberson, L.; Balinov, B.; Hagelin, G.; Dugstad, H.; Thomassen, T.; Forngren, B.H.; Forngren, T.; Hartvig, P.; Markides, K.; Yngve, U.; et al. Formation of Hydroxyl Spin Adducts via Nucleophilic Addition–Oxidation to 5,5-Dimethyl-1-pyrroline N-Oxide (DMPO). *Acta Chem. Scand.* **1999**, *53*, 584–593. [CrossRef]
19. Forrester, A.R.; Hepburn, S.P. Spin traps. A cautionary note. *J. Chem. Soc. C Org.* **1971**, 701–703. [CrossRef]
20. Hanna, P.M.; Chamulitrat, W.; Mason, R.P. When are metal ion-dependent hydroxyl and alkoxyl radical adducts of 5,5-dimethyl-1-pyrroline N-oxide artifacts? *Arch. Biochem. Biophys.* **1992**, *296*, 640–644. [CrossRef]
21. Romo, A.I.B.; Dibo, V.S.; Abreu, D.S.; Carepo, M.S.P.; Neira, A.C.; Castillo, I.; Lemus, L.; Nascimento, O.R.; Bernhardt, P.V.; Sousa, E.H.S.; et al. Ascorbyl and hydroxyl radical generation mediated by a copper complex adsorbed on gold. *Dalton Trans.* **2019**, *48*, 14128–14137. [CrossRef]
22. Villamena, F.A.; Hadad, C.M.; Zweier, J.L. Kinetic Study and Theoretical Analysis of Hydroxyl Radical Trapping and Spin Adduct Decay of Alkoxycarbonyl and Dialkoxyphosphoryl Nitrones in Aqueous Media. *J. Phys. Chem. A* **2003**, *107*, 4407–4414. [CrossRef]
23. Meissner, G.; Henglein, A.; Beck, G. Pulsradiolytische Untersuchung von Dimethylthioäther und Dimethylsulfoxyd in wäßriger Lösung. *Z. Für Nat. B* **1967**, *22*, 13–19. [CrossRef]
24. Dorfman, L.M.; Adams, G.E. *Reactivity of the Hydroxyl Radical in Aqueous Solutions*; National Standard Reference Data System; U.S. Department of Commerce-National Bureau of Standards: Washington, DC, USA, 1973; Volume 46.
25. Cederbaum, A.I.; Dicker, E.; Rubin, E.; Cohen, G. The effect of dimethylsulfoxide and other hydroxyl radical scavengers on the oxidation of ethanol by rat liver microsomes. *Biochem. Biophys. Res. Commun.* **1977**, *78*, 1254–1262. [CrossRef]
26. Anbar, M.; Neta, P. A compilation of specific bimolecular rate constants for the reactions of hydrated electrons, hydrogen atoms and hydroxyl radicals with inorganic and organic compounds in aqueous solution. *Int. J. Appl. Radiat. Isot.* **1967**, *18*, 493–523. [CrossRef]
27. Duling, D.R. Simulation of multiple isotropic spin-trap EPR spectra. *J. Magn. Reson. B* **1994**, *104*, 105–110. [CrossRef] [PubMed]

28. SimEPR Manual. Available online: http://www.niehs.nih.gov/research/resources/software/tox-pharm/tools/simepr/index.cfm (accessed on 23 May 2016).
29. Stoll, S.; Schweiger, A. EasySpin, a comprehensive software package for spectral simulation and analysis in EPR. *J. Magn. Reson.* **2006**, *178*, 42–55. [CrossRef]
30. Molton, F. Simultispin: A versatile graphical user interface for the simulation of solid-state continuous wave EPR spectra. *Magn. Reson. Chem.* **2020**, *58*, 718–726. [CrossRef]
31. Zalibera, M.; Rapta, P.; Staško, A.; Brindzová, L.; Brezová, V. Thermal generation of stable spin trap adducts with super-hyperfine structure in their EPR spectra: An alternative EPR spin trapping assay for radical scavenging capacity determination in dimethylsulphoxide. *Free Radic. Res.* **2009**, *43*, 457–469. [CrossRef]
32. Dvoranová, D.; Barbieriková, Z.; Brezová, V. Radical intermediates in photoinduced reactions on TiO_2 (an EPR spin trapping study). *Molecules* **2014**, *19*, 17279–17304. [CrossRef]
33. Mossoba, M.M.; Makino, K.; Riesz, P.; Perkins, R.C. Long-range proton hyperfine coupling in alicyclic nitroxide radicals by electron paramagnetic resonance. *J. Phys. Chem.* **1984**, *88*, 4717–4723. [CrossRef]
34. Finkelstein, E.; Rosen, G.M.; Rauckman, E.J. Spin trapping. Kinetics of the reaction of superoxide and hydroxyl radicals with nitrones. *J. Am. Chem. Soc.* **1980**, *102*, 4994–4999. [CrossRef]
35. Legge, R.L.; Thompson, J.E.; Baker, J.E. Free radical-mediated formation of ethylene from 1-aminocyclopropane-1-carboxylic acid: A spin-trap study. *Plant Cell Physiol* **1982**, *23*, 171–177.
36. Gilbert, B.C.; Silvester, S.; Walton, P.H. Spectroscopic, kinetic and mechanistic studies of the influence of ligand and substrate concentration on the activation by peroxides of CuI–thiolate and other CuI complexes. *J. Chem. Soc. Perkin Trans.* **1999**, *2*, 1115–1122. [CrossRef]
37. Bhattacharjee, S.; Deterding, L.J.; Chatterjee, S.; Jiang, J.; Ehrenshaft, M.; Lardinois, O.; Ramirez, D.C.; Tomer, K.B.; Mason, R.P. Site-specific radical formation in DNA induced by Cu(II)–H_2O_2 oxidizing system, using ESR, immuno-spin trapping, LC-MS, and MS/MS. *Free Radic. Biol. Med.* **2011**, *50*, 1536–1545. [CrossRef] [PubMed]
38. Nerud, F.; Baldrian, P.; Gabriel, J.; Ogbeifun, D. Decolorization of synthetic dyes by the Fenton reagent and the Cu/pyridine/H_2O_2 system. *Chemosphere* **2001**, *44*, 957–961. [CrossRef]
39. Sippola, V.O.; Krause, A.O.I. Bis(o-phenanthroline)copper-catalysed oxidation of lignin model compounds for oxygen bleaching of pulp. *Catal. Today* **2005**, *100*, 237–242. [CrossRef]
40. Korpi, H.; Figiel, P.J.; Lankinen, E.; Ryan, P.; Leskelä, M.; Repo, T. On in situ prepared Cu–Phenanthroline complexes in aqueous alkaline solutions and their use in the catalytic oxidation of veratryl alcohol. *Eur. J. Inorg. Chem.* **2007**, *2007*, 2465–2471. [CrossRef]
41. Gueneau, B.; Marlin, N.; Deronzier, A.; Lachenal, D. Pulp delignification with oxygen and copper(II)-polyimine complexes. *Holzforschung* **2014**, 68. [CrossRef]
42. Walger, E.; Khairumuzdanial, M.; Marlin, N.; Mortha, G.; Molton, F.; Duboc, C. Use of copper(II)-phenanthroline as a hydrogen peroxide activator for dyed pulp color-stripping—Investigation of the chemical mechanism. In Proceedings of the ISWFPC 2015 Proceedings, Vienna, Austria, 9–11 September 2015; Volume 2, pp. 250–253.